Photodissociation of the Hydroxymethyl Radical from the $2^2A''(3p_z)$ State: H₂CO and HCOH Products[†]

Lin Feng and Hanna Reisler*

Department of Chemistry, University of Southern California, Los Angeles, California 90089-0482

Received: May 12, 2004; In Final Form: June 17, 2004

The photodissociation of the hydroxymethyl radical in excited vibrational levels of the Rydberg $3p_z$ state is investigated by the core-sampling time-of-flight method and infrared-ultraviolet (IR+UV) double resonance ionization spectroscopy. Translational energy distributions of dissociation products of CH₂OD ($3p_z$; v) are measured for selected vibrational levels. CH₂OD → D + CH₂O (I) and CH₂OD → H + CHOD (II) are identified as major dissociation channels. Secondary dissociation from internally excited H₂CO and HCOD photofragments is observed when their internal energy exceeds the threshold for H/D formation. Mechanisms for secondary H/D production include direct dissociation and dissociation following HCOD ↔ HDCO isomerization. Several new overtone and combination bands of the $2^2A''(3p_z)$ ← $1^2A''$ transition of CH₂OH are accessed by IR+UV double resonance spectroscopy. Initial vibrational excitation of ground-state CH₂OH enhances the Franck−Condon factors for subsequent electronic transitions to the $3p_z$ state. Lifetime broadening is observed for all levels in the $3p_z$ state and the linewidth increases gradually with excitation energy from 11 cm⁻¹ for the origin band to 65 cm⁻¹ for the first overtone of the OH stretch. The broadening originates in increasingly efficient nonadiabatic couplings to other states.

I. Introduction

The importance of the hydroxymethyl radical (CH₂OH) in atmospheric and combustion environments has motivated intensive studies of its photochemistry.[1−5] The 3s, $3p_x$, $3p_y$, and $3p_z$ Rydberg states are the lowest excited states.[6−8] The $3p_x$ and $3p_z$ Rydberg states are bound, and their potential energy surfaces (PES) resemble that of the ground-state CH₂OH⁺ radical ion.[4] Among these four states, only $3p_y$ does not carry oscillator strength, and the spectroscopy involving transitions to the other states has been recently studied in molecular beams.[4,9−13]

It is intriguing that in going from the highest $3p_z$ to the 3s state the spectral features are increasingly broadened.[9,13] The origin band transition to the $3p_z$ state is the narrowest, with a 11 cm⁻¹ homogeneous linewidth, while the spectrum of the 3s state is featureless. All of these states are predissociative with lifetimes less than a picosecond.

Previous investigations of the UV photochemistry of CH₂-OD included measurements of translational energy and angular distributions of H and/or D photoproducts following excitation to the onset of the 3*s* state and the origin bands of the $3p_x$ and $3p_z$ states. These studies elucidated dissociation mechanisms[14−17] and, when combined with conical intersections calculations,[18] demonstrated that the Rydberg states under investigation are coupled to lower lying states. The final dissociation step takes place on the ground state, reached through 3s/ground-state conical intersections along the CH and OH coordinates.[18]

Several distinct vibrational levels in the $3p_z$ state were accessed by resonance-enhanced multiphoton ionization (REMPI) spectroscopy.[4,9] These included vibrational modes ν_4-ν_9 and their combination bands. However, only the origin band was investigated with respect to dissociation, and two

major channels were identified:[14,17]

$$CH_2OD \rightarrow CH_2O + D \qquad \Delta H = 1.32 \pm 0.07 \text{ eV} \quad \text{(I)}$$

$$CH_2OD \rightarrow HCOD + H \qquad \Delta H = 3.4 \pm 0.1 \text{ eV} \quad \text{(II)}$$

These channels were observed also in excitation to the 3s and $3p_x$ states, with reaction II first appearing near its energetic threshold.[16,17]

In this work, we extend the previous studies to photodissociation dynamics of CH₂OD from selected vibronic levels of the $3p_z$ state, e.g. 0_0^0, 4_0^1, 6_0^2. In addition to channels (I) and (II), secondary dissociation of CH₂O and HCOD fragments is observed following excitation to the 4_0^1 and 6_0^2 bands, as evidenced by the appearance of a second peak of slow D or H in the product translational energy distributions.

The OH (ν_1) and CH (ν_2 and ν_3) stretch modes in the $3p_z$ state of CH₂OH are important in the dissociation dynamics as they constitute reaction coordinates for channel (I) and (II), respectively.[18] Excited vibrational levels in the $3p_z$ state involving these modes were not detected previously by REMPI,[4,9] because of small Franck−Condon (FC) factors in excitation from the vibrationless level in the ground state. Recently, we reported infrared spectroscopy involving OH and CH stretch modes in the ground state of CH₂OH.[19] By carrying out IR+UV double resonance experiments, new vibrational levels in the $3p_z$ state were also directly observed. In these experiments, a FC-favorable transition to a selected vibrational level in the $3p_z$ state is accessed by preparing a suitable vibrational level in the ground state prior to UV excitation. The dissociation dynamics from the new levels has been inferred from spectral analyses. For example, the transition to the first overtone of the OH stretch is broadened considerably, indicating a shorter lifetime than that of lower energy vibrational levels in the $3p_z$ state.

---

* To whom correspondence should be addressed. E-mail: reisler@usc.edu.

II. Experimental Details

The radical generation procedure and experimental arrangement have been described in detail previously and will be briefly summarized here.[9,14] A mixture of 4% CH_3OD or CH_3OH (Aldrich, used without further purification) and ~1% Cl_2 (Air gas, 99.5%) in He at 2 atm total pressure in a 4 L glass bulb is prepared. This mixture is delivered to the radical generation chamber by a piezoelectrically driven pulsed nozzle operating at 10 Hz. A 355 nm laser pulse beam (Spectra Physics, GCR-11; 8 mJ, focused by a 30 cm f.l. cylindrical lens) crosses the edge of a 1-mm diameter quartz tube attached in front of the nozzle orifice. The radiation dissociates Cl_2, and the Cl atoms react rapidly with CH_3OD (CH_3OH), creating CH_2OD(CH_2OH).

The CH_2OD(CH_2OH) radicals undergo further cooling during the supersonic expansion. They pass through a 1.51 mm diameter skimmer (Beam Dynamics), and reach the photodissociation region vibrationally cold. A ~ 10 K rotational temperature is estimated from the $1+1'$ two-color REMPI spectrum obtained via the $3p_z$ state.[9]

A. Photofragment Yield (PFY) Spectra of H Atoms from CH_2OD. In this experiment, the CH_2OD radical beam is intersected with a UV pump beam whose frequency is scanned over the region of interest. The pump laser radiation excites the radicals to the $3p_z$ Rydberg states and then further ionizes them. A counterpropagating probe laser beam whose wavelength is fixed at ~121.6 nm is set to detect H atoms by $1+1'$ two-color REMPI via the L-α transition. The UV pump radiation is obtained from a seeded Nd:YAG laser-pumped OPO/OPA (Continuum, PL8000/Sunlite/FX-1; 0.5 mJ, 40 cm f.l. lens) system. The VUV probe laser radiation is generated in a tripling cell with a mixture of Kr and Ar, in which the doubled output (~ 365 nm, 2 mJ) of a Nd:YAG pumped dye laser system (Continuum, PL8010/ND6000, LDS 751) is tripled. The delay time between pump and probe laser firings is set at ~ 1 ns.

B. Core-Sampling Time-of-Flight of H and D Photofragments from CH_2OD. Time-of-flight (TOF) distributions of H and D photofragments from CH_2OD are recorded by the core-sampling technique combined with REMPI detection. This method has been described in detail elsewhere.[14,20] In brief, the core-sampling arrangement consists of a two-stage ion acceleration region, an 18 cm field-free drift region and a 4-mm diameter aperture installed in front of a multichannel plate detector (MCP, Galileo, 25 mm). The ion detector is positioned parallel to the plane defined by the molecular and laser beams. The aperture is mounted on a linear motion feedthrough (MDC, BLM-133-4) to allow alternation between total ion collection and core sampling. The core sampling technique utilizes a spatial restriction in the ion detection to eliminate contributions from off-axis ions, thereby yielding the speed distribution of the recoiling fragments in a straightforward manner.

TOF spectra of H or D products are recorded under the core-sampling conditions, in which the frequency of the pump laser beam is fixed at the peak of the transition to a vibrational level in the $3p_z$ state and that of the probe laser is set at the center of the Doppler profile of the H or D photofragment. Each set of spectra are recorded with the pump laser polarization parallel and perpendicular to the TOF axis. The alternation of the polarization is accomplished by controlling the time delay between the triggering of the pump laser pulse and a photoelastic modulator (PEM-80, HINDS International, Inc.). The pump and probe laser beams are generated by the same laser systems used in H atom PFY experiment. The procedure of transforming the measured TOF profile into kinetic energy distribution $P(E_T)$ has been described in detail elsewhere.[14,20]
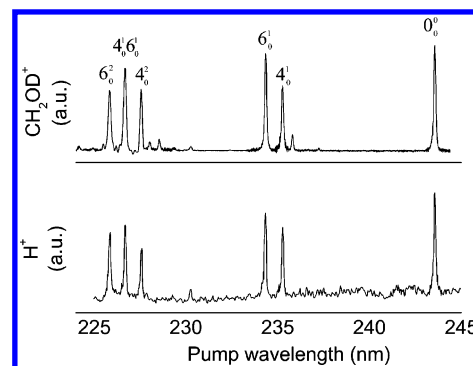

Figure 1. $1+1'$ REMPI spectrum (upper panel) and H photofragment yield spectrum (lower panel) of CH_2OD. Assignments are from ref 9.

C. IR+UV Double Resonance Ionization of CH_2OH. In these experiments, the IR laser beam frequency is fixed at the center of a transition to a selected rovibrational level of the OH− or CH− stretch mode in the ground state, whereas the UV frequency is scanned in the energy region around 41 062 cm^{-1}, i.e., the peak of the origin band of the CH_2OH $2^2A''(3p_z)$ ← $1^2A''$ transition.[9] IR radiation (4 mJ, 20 cm f.l. lens) is obtained from a seeded Nd:YAG pumped OPO/OPA (LaserVision) and UV radiation is obtained from another seeded Nd:YAG pumped OPO/OPA (Continuum, PL8000/Sunlite/FX-1; 1.0 mJ, 40 cm f.l. lens) system. The spectra are recorded in both "IR on" and "IR off" conditions. In "IR on" conditions, the probe laser is fired 20 ns after the pump laser, whereas with "IR off", the probe laser precedes the pump laser by 1 μs. The time delay is regulated by Labview controlled digital pulse/delay generators (DG 535, Stanford Research Systems, 5 ps resolution).

III. Results

A. REMPI and H-Atom PFY Spectra of CH_2OD. Several vibrational levels in the $3p_z$ state of CH_2OD have been previously characterized by REMPI spectroscopy in a flow reactor and molecular beam.[4,9] We have reproduced the $1+1'$ REMPI spectrum via the $2^2A''(3p_z)$ ← $1^2A''$ transition, and our results are shown in the top panel of Figure 1. The two strong progressions have been assigned as 6_0^n (CO stretch) and 4_0^n (CH$_2$ scissors), $n = 0$ and 1, by Johnson and Hudgens[4] and Aristov et al.[9]

A PFY spectrum of H atoms is recorded in the same energy region of the REMPI spectrum of CH_2OD and shown in Figure 1. In this experiment, the frequency of the pump laser is scanned, whereas that of the probe laser is fixed at the peak of the detection line of the H atom. The clear correspondence between the H−PFY and CH_2OD REMPI spectral features indicates that H atom is a product of the dissociation of CH_2OD ($3p_z$). Combined with the D photofragment yield spectrum reported previously by Conroy et al. in the same energy region,[14] we conclude that both H and D are produced in dissociation from the vibrational levels of $3p_z$ examined here.

B. Translational Energy Distributions of D and H Channels of CH_2OD. Figure 2, panels b and c, shows translational energy distributions, $P(E_T)$'s, of the D (top panel) and H (bottom panel) channels [reactions I and II, respectively] obtained from core-sampling TOF profiles following excitation to the 4_0^1 (CH$_2$ scissors, 5.26 eV) and 6_0^2 (CO stretch, 5.47 eV) bands of CH_2OD. For comparison, $P(E_T)$ of the same channels following excitation to the 0_0^0 band (5.08 eV) are also displayed (Figure 2a).

In these experiments, the pump laser frequency is fixed at the peak of each band, whereas that of the probe laser is set at
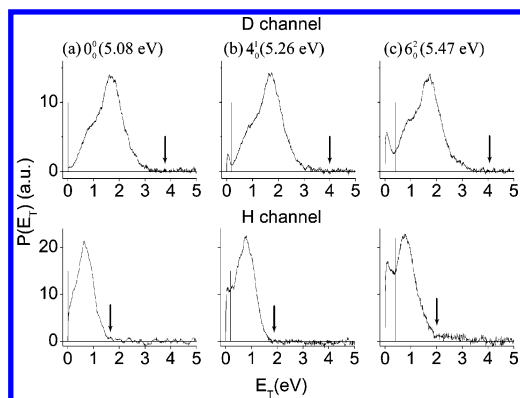
Photodissociation of the Hydroxymethyl Radical

J. Phys. Chem. A, Vol. 108, No. 45, 2004 **9849**

Figure 2. c.m. E_T distributions obtained by monitoring D (upper panels) and H (bottom panels) fragments from dissociation of (a) 0_0^0 (5.08 eV), (b) 4_0^1 (CH₂ scissors, 5.26 eV), and (c) 6_0^2 (CO stretch, 5.47 eV) bands in the $3p_z$ state of CH₂OD. The arrow in each panel indicates the calculated kinetic energy limit associated with reactionl I (upper panels) or II (bottom panels). The solid line in each panel marks the value of the translational energy below which CH₂O carries sufficient internal energy to dissociate to H + HCO.
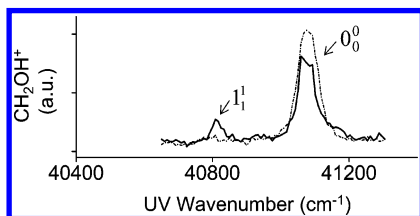

Figure 3. IR+UV double resonance spectrum of CH₂OH via the $3p_z$ state with IR off (dot dashed line) and IR tuned to the OH stretch at 3674.3 cm⁻¹ (solid line).

the center of the Doppler profile of the D and H photofragment. Each result is shown after background subtraction taken by tuning the pump laser frequency off resonance. Through this subtraction procedure, the contributions of D and H background from the radical generation process are minimized.

C. IR+UV Double Resonance Spectroscopy. An example of an IR + UV double resonance spectrum is shown in Figure 3. This spectrum is obtained by fixing the IR frequency at 3674.3 cm⁻¹ [$^qQ_1(2)$] to pump CH₂OH to a single rovibrational level of the fundamental OH stretch (ν_1) in the ground state, while scanning the UV frequency. The assignment of the rovibrational level in the ground state is based on ref 19. The solid and dot dashed lines represent "IR-on" and "IR-off" spectra, respectively. The 0_0^0 transition, slightly saturated in our spectrum, is the dominant feature. It is observed in both "IR-off" and "IR-on" spectra, with the intensity in the "IR-on" spectrum reduced by depletion of ground-state population by IR absorption. A new vibrational level to the red of the origin band (0_0^0) is evident in the "IR-on" spectrum. The absence of this peak in the "IR-off" spectrum suggests that it is associated with the rovibrational level excited in the IR. Similar spectra, shown in ref 19, are obtained by varying the IR frequency and accessing selected rovibrational levels of the fundamental CH symmetric stretch (ν_3) at 3048.9 cm⁻¹ [$^qR_1(2)$], CH asymmetric stretch (ν_2) at 3170.5 cm⁻¹ [$^rR_0(1)$], and the first OH-stretch overtone ($2\nu_1$) at 7159.7 cm⁻¹ [$^rP_0(2)$].[19] The additional transitions and their assignments are shown in Figure 4.

IV. Discussion

A. CH₂O and HCOD Products from CH₂OD (3p$_z$). As shown in Figure 2, the translational energy distributions of the D and H channels obtained by exciting the 0_0^0, 4_0^1, and 6_0^2 bands
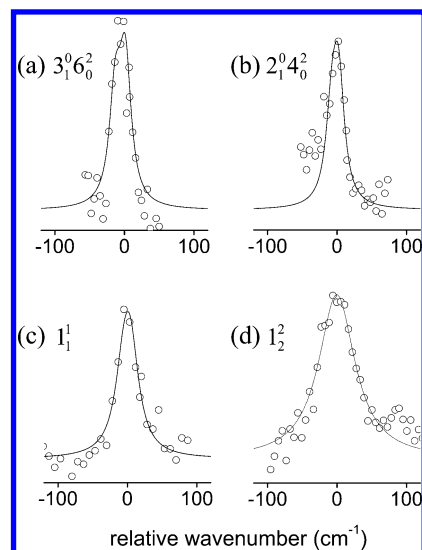

Figure 4. CH₂OH absorption bands (open circles) (a) $3_1^0 6_0^2$, (b) $2_1^0 4_0^2$, (c) 1_1^1, and (d) 1_2^2 of the $2^2A''(3p_z) \leftarrow 1^2A''$ transition. The spectra in (a), (b), (c), and (d) are shifted by 3228, 2967, 3408, and 6639 cm⁻¹, respectively, relative to the 0_0^0 band (41 062 cm⁻¹). Spectral fits (Lorentzian lineshape) are shown as solid lines. The upper state rotational constants used are (in cm⁻¹) $A_1 = 6.70$, $\bar{B}_0 = 1.08$. The lower state rotational constants are (in cm⁻¹) (a) $A_0 = 6.48$, $\bar{B}_0 = 0.93$; (b) $A_0 = 6.41$, $\bar{B}_0 = 0.93$; (c) $A_0 = 6.41$, $\bar{B}_0 = 0.92$; (d) $A_0 = 6.39$, $\bar{B}_0 = 0.93$.

are similar in shape in the region of high translational energy. It has been previously shown that excitation in the origin band gives rise to D and H products from channels (I) CH₂OD → D + CH₂O and (II) CH₂OD → H + CHOD, respectively.[17] The measured H/D ratio was 1.0 ± 0.2 for the origin band. Its value increases smoothly in the energy region covering absorption to the 3s, 3p$_x$, and 3p$_z$ states. No sharp change was detected when the band origins of the transitions to the 3p$_x$ and 3p$_z$ states were reached, indicating the existence of a common final step in the dissociation following excitation to the 3s, 3p$_x$, and 3p$_z$ states. The translational energy limits associated with production of CH₂O and CHOD are marked by arrows in Figure 2. The consistency of these limits with the observations indicates that channels (I) and (II) are major pathways in the dissociation from the 4_0^1 and 6_0^2 bands as well.

Unlike the results from the 0_0^0 band, however, a second peak at low translational energy begins to develop in the P(E_T)'s of the D and H channels obtained via excitation to the 4_0^1 band (Figure 2b), and its intensity increases with increasing excitation energy. An example is shown in Figure 2c obtained via excitation to the 6_0^2 band. Caution has been exercised in ascertaining that these peaks do not represent artifacts of the core sampling technique in the region of small recoil. It is well-known that the core-sampling assumption breaks down when $v \leq r_{core}/t$, where r_{core} is the core radius and t is the time-of-flight of ions reaching the core region. This breakdown leads to a large increase in collection efficiency at low E_T, and thus enhancement of signal intensity. In our experimental arrangement, the translational energy corresponding to the breakdown of core-sampling is 0.02 eV, a value that is almost an order of magnitude smaller than the translational energy of the peaks of the slow features. In addition, even though the experimental conditions are the same for all the measured vibrational levels shown in Figure 2, the slow peak is observed only following 4_0^1 and 6_0^2 excitations and its width increases with the increase in excitation energy. This confirms that the slow peak represents a change in mechanism rather than an experimental artifact.

Although quantitative evaluations of $P(E_T)$ are not secure in the low E_T region, qualitative conclusions can still be drawn by comparing distributions from different vibrational levels in the $3p_z$ state.

We believe that the slow peaks arise from secondary dissociation of "hot" H_2CO and HCOD generated by reactions I and II, respectively. The $P(E_T)$'s of products from the 0_0^0 band (Figure 2a) indicate that CH_2O and HCOD fragments with large amounts of internal excitation are produced. These fragments further dissociate when their internal energy exceeds the dissociation thresholds to H(D) +D(H)CO, i.e., the radical channel of formaldehyde and hydroxymethylene dissociation.

Referring to Figure 2, we notice that slow components appear in the $P(E_T)$'s of both D and H atoms. Secondary D fragments can be generated only via dissociation of HCOD products, either directly or following isomerization, whereas slow H atoms can originate in dissociation of both CH_2O and HCOD. Secondary dissociation is not observed in the dissociation via the 0_0^0 band of CH_2OD, in accordance with energy conservation: no CH_2O and CHOD fragments carrying sufficient internal energy for dissociation to H/D can be produced at this excitation energy. The exact position of the slow peak in the bottom panels is hard to discern, because this feature is partially overlapped by the primary feature of the H channel, which is centered at low translational energies. Nevertheless, all of the slow peaks can be associated energetically with secondary dissociation of CH_2O or HCOD/CHDO products. The solid line in each panel in Figure 2 indicates the value of the translational energy below which CH_2O fragments carry sufficient internal energy to dissociate to H + HCO.[21] The consistency of these values with the onsets of the slow H/D peaks in all the panels suggests that secondary dissociation of CH_2O and CHOD takes place, giving rise to slow H and D atoms.

To further assess the sources of slow H and D products, as well as the role of $H_2CO \leftrightarrow HCOH$ isomerization, we discuss here briefly additional information relevant to the unimolecular reactions of these two isomers. Features of the H_2CO PES have been extensively explored previously, revealing that H_2 + CO and H + HCO are the main dissociation pathways on the S_0 PES.[22–27] The barrier to H_2 + CO has been calculated by various methods,[23,24,28–37] and experimental work by Polik et al. places it at 3.41 eV,[38] whereas the H + HCO pathway is barrierless and its dissociation threshold is 3.75 eV.[27,39] Because of the loose transition state of the radical channel, its importance relative to the H_2 + CO channel increases with increasing excitation energy.

To the best of our knowledge, experimental studies of the dissociation of HCOH have not been reported. Previous theoretical calculations by Goddard and Schaefer show that the trans conformer of hydroxycarbene lies slightly below the cis form, and the isomerization barrier from *trans*-hydroxycarbene to formaldehyde is ~1.56 eV.[24] This corresponds to a barrier of ~3.68 eV relative to CH_2O, a value close to the dissociation threshold of $CH_2O \rightarrow$ H + HCO (3.75 eV). In more recent studies,[25,39–42] the relevant energies were recalculated, and it was found that (i) the barrier to isomerization is comparable to but slightly lower than the energy threshold to direct H_2CO dissociation (e.g., 1.3 vs 1.5 eV),[39,41] and (ii) H_2CO lies much lower in energy than *cis,trans*-HCOH (by 2.2–2.4 eV).[25,39,40] Therefore, dissociation of HCOH(D) via isomerization is a possible pathway for H(D) formation:

$$cis,trans\text{-HCOH} \underset{k_{-1}}{\overset{k_1}{\rightleftharpoons}} H_2CO \rightarrow H + CHO$$
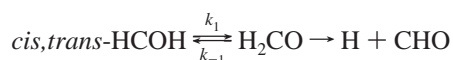
Although the transition state for the radical channel of H_2CO is loose (located at >3 Å), Reid et al. find in their ab initio calculations that the transition state for *cis,trans* HCOH → H + HCO is much tighter (<2 Å).[42] In fact, their calculations indicate a distinct barrier for dissociation of the trans isomer. Reid et al. argue convincingly that the tightness of the transition state and the existence of the barrier result from avoided crossings of electronic states that lead to the adiabatic S_0 and S_1 states of HCOH. Therefore, at energies close to the dissociation threshold the direct dissociation rate of HCOH may be sufficiently slow to allow isomerization to H_2CO, which has a deep well. Bauerfeldt et al. calculated the microcanonical rate coefficients $k(E,J)$ for the $H_2CO \rightarrow H_2$ + CO, $H_2CO \rightarrow$ H + HCO, and $H_2CO \rightarrow$ *trans*-HCOH paths in a range of energy from 0 to 0.7 eV above the barrier of formaldehyde isomerization,[25] which covers the energy region examined here. The calculations show that the three unimolecular paths compete at these energies. The rate constants calculated by classical trajectories and Rice-Ramsperger-Kassel-Marcus (RRKM) theory show that the rate constant of the forward reaction (k_1) is larger than the reverse one (k_{-1}) by nearly an order of magnitude at low excess energies, as expected by the energetics.[40] Thus, we argue that near the dissociation threshold HCOD isomerization to CHDO is an additional source of slow H and D products. A more complete experimental and theoretical study of the dissociation of CHOH will help in further clarifying the roles of direct dissociation and dissociation via isomerization.

Additional evidence for the production of "hot" formaldehyde in dissociation of CH_2OD ($3p_z$) is provided by the observation of secondary CO products. Previously, we reported that CO products in v = 0 and 1 were observed in photodissociation of CH_2OD at 230.1 nm (5.37 eV).[16] In this one-color experiment, we used (2+1) REMPI via the CO ($B^1\Sigma^+$) state to detect CO ($X^1\Sigma^+$). The detection wavelength coincided with a $2^2A''(3p_z)$ ← $1^2A''$ absorption band of CH_2OD, and we interpreted the observed CO (v = 0,1) signals as arising from secondary dissociation of CH_2O.

We cannot exclude some contribution to the slow D and H peaks from isomerization of the CH_2OD precursor followed by dissociation. The isomerization of CH_2OD to CH_2DO may give rise to "hot" CH_2O and CHDO fragments. No evidence for such isomerization was found experimentally in dissociation from the 3s and $3p_x$ states of CH_2OD.[16,17] However, a small contribution (~10%) from the isomerization pathway has been estimated by Harding in the CH_2 + OD reaction that evolves via a CH_2OD intermediate.[41] The initial energy of 5.4 eV used in the calculations is close to the energies of the vibrational levels in $3p_z$ reported here.

In summary, the photodissociation of CH_2OD via the 0_0^0, 4_0^1, and 6_0^2 levels of the $3p_z$ state gives rise to highly internally excited CH_2O and HCOD. Secondary dissociation of these fragments is the likely source of the slow peaks in the H and D translational energy distributions. Based on previous results, the predissociation mechanism from the $3p_z$ state probably involves conical intersections along the OH and CH coordinates.[17,18] Sequential conical intersections with lower Rydberg states may explain why products generated via the $3p_z$ state are internally hot, whereas dissociation following excitation to the lower 3s and $3p_x$ states gives rise to products with a larger fraction of energy disposed in translation.[16,17] Symmetry considerations dictate that in the initial coupling between the $2^2A''(3p_z)$ state and lower Rydberg states of A′ symmetry, out-of-plane modes must be involved. Such modes may propagate through the sequence of internal conversions that precede the final 3s/

Photodissociation of the Hydroxymethyl Radical

J. Phys. Chem. A, Vol. 108, No. 45, 2004 **9851**

TABLE 1: Experimentally Determined and Theoretically Calculated Vibrational Frequencies of Levels in the $3p_z$ State of CH_2OH, Their Linewidths, and Lifetimes

transition	vibrational mode in the $3p_z$ state	frequency[a] (cm^{-1})		linewidth (cm^{-1})	lifetime (fs)
		ν_{obs}	ν_{calc}[b]		
$3_1^0 6_0^2$	ν_6(CO stretch)=2	3228	3286	20 ± 1	265 ± 13
$2_1^0 4_0^2$	ν_4(CH$_2$ scissors)=2	2967	2926	20 ± 2	260 ± 25
1_1^1	ν_1(OH stretch)=1	3408	3511	30 ± 3	177 ± 18
1_2^2	ν_1(OH stretch)=2	6639	7022	65 ± 5	82 ± 6

[a] Error bar: ± 5 cm^{-1}. [b] From ref 4.

ground-state conical intersections located in the repulsive part of the PES. The radicals undergoing such multiple intersections may carry a large amount of internal energy in out-of-plane modes (torsion and CH$_2$ wag) as they reach the final dissociation step on the ground PES, leading finally to "hot" products.

Examining dissociation from vibrations along the OH (ν_1)- or CH (ν_2 and ν_3)- stretch modes may provide additional insight into surface couplings and dissociation mechanisms. Unfortunately, these modes in the $3p_z$ state are not easily accessed because of unfavorable FC factors with the vibrationally unexcited ground state. This encouraged us to search for these levels by vibrationally mediated IR+UV double resonance spectroscopy.

B. Lifetimes and Vibrationally Mediated Spectroscopy of CH_2OH. No vibronic bands involving ν_1-ν_3 modes were observed in the REMPI spectrum shown in Figure 1. This can be explained by comparing the geometries of the radical's ground and $3p_z$ states. The equilibrium geometries of the ground-state radical and cation were calculated ab initio.[4,7,8] Since Rydberg orbitals are large and diffuse, the geometries of the cation and neutral Rydberg states are similar to a good approximation. The calculations show that the main geometry change in going from the neutral to the cation involves a 0.12 Å decrease in CO bond distance, consistent with a progression in the CO stretch (ν_6) observed in the REMPI spectrum. The OH bond distance changes by only 0.02 Å and the two C−H bond distances change by less than 0.01 Å.

Considering the small OH and CH bond distance changes, $\Delta v = 0$ sequences are expected in excitation of the ν_1−ν_3 modes to Rydberg states, explaining the absence of these modes in the REMPI spectrum obtained in the molecular beam. Vibrational levels of these modes in the $3p_z$ Rydberg state can be accessed, however, by prior vibrational excitation in the ground state.

To this end, we exploited the method developed for studying IR transitions to the OH and CH stretch vibrations in the ground state of CH_2OH.[19] By first preparing CH_2OH in vibrationally excited levels on the ground state, FC factors for selected transition to the $3p_z$ state could be enhanced. The vibrational frequencies in $3p_z$ are derived from the IR+UV double resonance transition frequencies by using the relation

$$n\nu_i(3p_z) = \nu_{IR} + \nu_{UV} - \nu(3p_z(0_0^0)) \qquad (1)$$

The corresponding assignments and band center frequencies for the peaks shown in Figure 4 are listed in Table 1 and compared with calculated values. The frequencies of ν_2 and ν_3 calculated for the ground electronic states of the neutral and the cation differ by only ~50 cm^{-1}. Since the observed bandwidth (FWHM) of the 0_0^0 transition is greater than 50 cm^{-1}, the 2_1^1 and 3_1^1 peaks are obscured by the 0_0^0 peak. We did, however,

observe a slight enhancement in signal to the red of the 0_0^0 peak following excitation to ν_2 or ν_3 on the ground state in positions corresponding to the 2_1^1 and 3_1^1 transitions.[19] These overlapped bands are not considered further.

The $3_1^0 6_0^2$, $2_1^0 4_0^2$, 1_1^1, and 1_2^2 bands, however, are well separated from the 0_0^0 band and can be investigated. The 1_2^2 band is considerably broader than the $3_1^0 6_0^2$, $2_1^0 4_0^2$, and 1_1^1 transitions as evident from Figure 4. The homogeneous linewidths were estimated by simulating the spectra with a Lorentzian width as a fit parameter. The fit results are shown in Figure 4 as solid lines and the homogeneous linewidths that give the best fits are listed in Table 1.

We varied the IR and UV laser energies used in the IR + UV double resonance experiments. The broadness of the bands was independent of IR laser energy in the range 3−5 mJ and UV laser energy of 0.8−1.2 mJ. In addition, the $3_1^0 6_0^2$ band had the same total energy as the 6_0^2 band observed in the REMPI spectrum reported in ref 9, in which 0.2 mJ UV laser energy (focused with 100 cm f.l. lens) was used. The 6_0^2 band is best fit with a 20 ± 2 cm^{-1} linewidth, in good agreement with the value shown in Table 1. The similar linewidths obtained in the IR + UV double resonance and REMPI spectra suggests that power broadening is negligible.

In the simulations, the rotational constants of the lower state are fixed at the values determined in ref 19. Because we have no information on the change in geometry upon vibrational excitation in the $3p_z$ state, a rigid rotor approximation is used, and rotational constants of the upper state are calculated using the equilibrium geometry of the radical ion. The radical is treated as a prolate-top undergoing a parallel transition,[6,8,9] and the rotational constant $\bar{B}$ is taken as the average of the calculated asymmetric rotor rotational constants B and C. Note that only a single rovibrational level in the ground state is involved in the IR+UV double resonance spectra, while the 0_0^0 and 6_0^2 bands should be simulated with $T = 10$ K rotational temperature.

Comparing with the 11 cm^{-1} homogeneous linewidth of the 0_0^0 band (obtained under unsaturated conditions),[9] incremental increases in linewidth are observed with increasing vibrational energy in $3p_z$, with a 6-fold increase relative to 0_0^0 for the first overtone transition at 6639 cm^{-1}. This implies a large decrease in lifetime for the $\nu_1 = 2$ vibronic level in the $3p_z$ state (see Table 1).

Several factors can contribute to the shorter lifetime of the $2\nu_1$ level. As discussed above, we believe that dissociation from the $3p_z$ state involves multiple surface crossings.[17] The lifetime dependence on excitation energy in the $3p_z$ state is probably due to stronger overall coupling to modes that promote nonadiabatic transitions via conical intersections. The increase in the density of states with increasing vibrational energy may also lead to significant intramolecular vibrational redistribution (IVR) in $3p_z$, making crossing seams between $3p_z$ and lower Rydberg states more accessible. A similar behavior has been observed in the photodissociation of formaldehyde via T_1.[22] Mode-selective effects have not been found; they may be distinguished from merely energy effects in cases when nearly isoenergetic vibrational levels in the $3p_z$ state can be observed. It also remains for electronic structure calculations to further explore the $3p_z$ PES and especially its nonadiabatic couplings to other states.

V. Conclusions

The dissociation dynamics from several vibrational levels in the $3p_z$ states have been examined using both P(E_T) measure-

ments and spectroscopy analysis. Translational energy distributions of the D and H channels are obtained for dissociation from the 0_0^0, 4_0^1, and 6_0^2 levels in the $3p_z$ state of CH_2OD. In addition to the two major dissociation channels, $CH_2OD \rightarrow D + CH_2O$ and $CH_2OD \rightarrow H + CHOD$, observed for all the vibrational levels, secondary dissociation of CH_2O and $CHOD$ takes place following excitation to the 4_0^1 and 6_0^2 bands. CH_2O and $CHOD$ products carrying internal energy sufficient for dissociation give rise to $H(D) + D(H)CO$ fragments. Isomerization of $CHOD$ to $CHDO$ is found to be a possible pathway for dissociation of $CHOD$, in addition to direct dissociation to $D + HCO$.

1_1^1, 1_2^2, and two combination bands ($3_1^0 6_0^2$ and $2_1^0 4_0^2$) in CH_2-OH are identified in IR+UV double resonance spectra. A decrease in lifetime with increasing excitation energy is deduced from the homogeneous linewidth of these bands. This increase in predissociation rate is most likely a consequence of increasing coupling matrix elements to lower lying electronic states. The out-of-plane modes that promote the sequential surface couplings required for dissociation are probably also responsible for the large internal energy of the formaldehyde and hydroxymethylene products.

References and Notes

(1) Lin, J. J.; Shu, J.; Lee, Y. T.; Yang, X. *J. Chem. Phys.* **2000**, *113*, 5287.

(2) Shu, J.; Lin, J. J.; Lee, Y. T.; Yang, X. M. *J. Chem. Phys.* **2001**, *115*, 849.

(3) Pagsberg, P.; Munk, J.; Sillesen, A.; Anastasi, C. *Chem. Phys. Lett.* **1988**, *146*, 375.

(4) Johnson, R. D.; Hudgens, J. W. *J. Phys. Chem.* **1996**, *100*, 19874.

(5) Ahmed, M.; Peterka, D. S.; Suits, A. G. *Phys. Chem. Chem. Phys.* **2000**, *2*, 861.

(6) Rettrup, S.; Pagsberg, P.; Anastasi, C. *Chem. Phys.* **1988**, *122*, 45.

(7) Bruna, P. J.; Grein, F. *J. Phys. Chem. A* **1998**, *102*, 3141.

(8) Bruna, P. J.; Grein, F. *J. Phys. Chem. A* **2001**, *105*, 8599.

(9) Aristov, V.; Conroy, D.; Reisler, H. *Chem. Phys. Lett.* **2000**, *318*, 393.

(10) Dulcey, C. S.; Hudgens, J. W. *J. Phys. Chem.* **1983**, *87*, 2296.

(11) Dulcey, C. S.; Hudgens, J. W. *Bull. Soc. Chim. Belg.* **1983**, *92*, 583.

(12) Dulcey, C. S.; Hudgens, J. W. *J. Chem. Phys.* **1986**, *84*, 5262.

(13) Feng, L.; Huang, X.; Reisler, H. *J. Chem. Phys.* **2002**, *117*, 4820.

(14) Conroy, D.; Aristov, V.; Feng, L.; Reisler, H. *J. Phys. Chem. A* **2000**, *104*, 10288.

(15) Conroy, D.; Aristov, V.; Feng, L.; Sanov, A.; Reisler, H. *Acc. Chem. Res.* **2001**, *34*, 625.

(16) Feng, L.; Demyanenko, A. V.; Reisler, H. *J. Chem. Phys.* **2003**, *118*, 9623.

(17) Feng, L.; Demyanenko, A. V.; Reisler, H. *J. Chem. Phys.* **2004**, *120*, 6524.

(18) Hoffman, B. C.; Yarkony, D. R. *J. Chem. Phys.* **2002**, *116*, 8300.

(19) Feng, L.; Wei, J.; Reisler, H. *J. Phys. Chem. A* **2004**, in press.

(20) Syage, J. A. *J. Chem. Phys.* **1996**, *105*, 1007.

(21) The corresponding value for HCOD has been calculated by taking into account the isotope replacement. This difference is ignored in Figure 2, which is justified considering the low resolution of the core-sampling method at low E_T and the overlap of the fast and slow peaks.

(22) Valachovic, L. R.; Tuchler, M. F.; Dulligan, M.; Droz-Georget, T.; Zyrianov, M.; Kolessov, A.; Reisler, H.; Wittig, C. *J. Chem. Phys.* **2000**, *112*, 2752.

(23) Goddard, J. D.; Yamaguchi, Y.; Schaefer, H. F. *J. Chem. Phys.* **1981**, *75*, 3459.

(24) Goddard, J. D.; Schaefer, H. F. *J. Chem. Phys.* **1979**, *70*, 5117.

(25) Bauerfeldt, G. F.; de Albuquerque, L. M. M.; Arbilla, G.; da Silva, E. C. *J. Mol. Struct. (THEOCHEM)* **2002**, *580*, 147.

(26) Yonehara, T.; Kato, S. *J. Chem. Phys.* **2002**, *117*, 11131.

(27) Terentis, A. C.; Kable, S. H. *Chem. Phys. Lett.* **1996**, *258*, 626.

(28) Jaffe, R. L.; Hayes, D. M.; Morokuma, K. *J. Chem. Phys.* **1974**, *60*, 5108.

(29) Jaffe, R. L.; Morokuma, K. *J. Chem. Phys.* **1976**, *64*, 4881.

(30) Harding, L. B.; Schlegel, H. B.; Krishnan, R.; Pople, J. A. *J. Phys. Chem.* **1980**, *84*, 3394.

(31) Frisch, M. J.; Krishnan, R.; Pople, J. A. *J. Phys. Chem.* **1981**, *85*, 1467.

(32) Dupuis, M.; Lester, W. A.; Lengsfield, B. H.; Liu, B. *J. Chem. Phys.* **1983**, *79*, 6167.

(33) Frisch, M. J.; Binkley, J. S.; Schaefer, H. F. *J. Chem. Phys.* **1984**, *81*, 1882.

(34) Scuseria, G. E.; Schaefer, H. F. *J. Chem. Phys.* **1989**, *90*, 3629.

(35) Nakano, H.; Nakayama, K.; Hirao, K.; Dupuis, M. *J. Chem. Phys.* **1997**, *106*, 4912.

(36) Sung, B. J.; Kim, M. S. *J. Chem. Phys.* **2000**, *113*, 3098.

(37) Feller, D.; Dupuis, M.; Garrett, B. C. *J. Chem. Phys.* **2000**, *113*, 218.

(38) Polik, W. F.; Guyer, D. R.; Moore, C. B. *J. Chem. Phys.* **1990**, *92*, 3453.

(39) Klippenstein, S. private communication.

(40) Yonehara, T.; Kato, S. *J. Chem. Phys.* **2002**, *117*, 11131.

(41) Harding, L. B. private communication.

(42) Reid, D. L.; Hernandez-Trujillo, J.; Warkentin, J. *J. Phys. Chem. A* **2000**, *104*, 3398.